A quasi-Linear Parameter Varying (qLPV) Approach for Tiltrotor Conversion Modeling and Control Synthesis

Hafiz Noor Nabi
PhD Candidate
Politecnico di Milano & Delft University of Technology
Milan, Italy

Coen de Visser
Assistant Professor
Delft University of Technology
Delft, The Netherlands

Marilena D. Pavel
Assistant Professor
Delft University of Technology
Delft, The Netherlands

Giuseppe Quaranta
Associate Professor
Politecnico di Milano
Milan, Italy

ABSTRACT

A safe conversion of tiltrotor from helicopter mode to airplane mode is ensured through maneuvering within the conversion corridor, a constrained region in the airspeed versus nacelle angle graph. This paper presents preliminary work in the development of an automatic conversion maneuver. A high order quasi-Linear Parameter Varying model is developed for XV-15 that combines discrete state-space models to provide a varying model dynamics and trim characteristics during the conversion maneuver. Tracking control system based on gain scheduled linear quadratic tracker with integrator (LQTI) is designed for automatic conversion maneuver for XV-15 based on the qLPV model. Lastly, an optimization routine is performed to fly various conversion trajectories and identify optimal conversion maneuver.

NOTATION

*

$\mathbf{A}$	State matrix
$\mathbf{B}$	Control matrix
h	Altitude
K_r, K_t, K_i	Regulating, tracking and integral gains
q	Aircraft pitch rate
T_f	Final simulation time
u, w	Velocities in body x and z axes
V	Velocity
x_r, x_t	Regulating and tracking states
$\mathbf{u_{trim}}$, $\mathbf{x_{trim}}$	Trim control inputs and states
β_0, β_{1s}, β_{1c}	Conning, lateral and longitudinal rotor flapping
β_{Gs}, β_{Gc}	Lateral and longitudinal rotor gimbal
β_i	Nacelle incidence angle
δ_f	Wing flap angle
η_X, η_Y, η_Z	Bending of tip of wing pylon about X, Y and Z axes
$\rho(t)$	Scheduling parameter vector
τ	Time constant
θ	Aircraft pitch angle
θ_0, θ_{1s}, θ_{1c}	Collective pitch, longitudinal and lateral cyclic

Presented at the Vertical Flight Society 75th Annual Forum & Technology Display, Philadelphia, Pennsylvania, May 13–16, 2019.

INTRODUCTION

Tiltrotors can operate over a broad flight envelope. The ability to hover like a helicopter and at the same time to fly at relatively high cruise speeds and range like a fixed wing airplane make them an effective point-to-point fast means of transportation and are considered as the best solution for modern civil transportation system (Refs. 1, 2). Throughout their development, tiltrotor aircraft have been characterized by a high level of technological sophistication to enable their extensive flight envelope and to perform satisfactorily over a broad range of flight configurations.

The conversion maneuver that allows a tiltrotor to transform between helicopter and airplane mode is considered to be one of the most critical operations. A safe conversion is ensured by maneuvering within a constrained region in the airspeed versus nacelle angle graph, called the conversion corridor, illustrated in Figure 1 for the case of XV-15. The lower limit

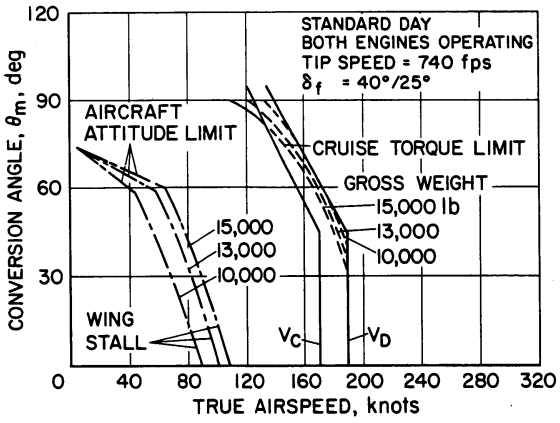

Fig. 1. XV-15 conversion corridor (Ref. 6)

of conversion corridor is defined by wing stall and pitch attitude whereas, the upper limit is characterized by power required and rotor blade flapping. Successful conversion from helicopter to airplane configuration is achieved, at constant altitude, when increase in wing lift matches the reduction in lift generated by rotors. Currently, the conversion maneuver is managed by the pilot and in general the pilot workload is higher than in other phases of flight, in particular, the handling quality ratings degrade at higher nacelle tilt rate (Ref. 3). This situation may not be optimal in particular, considering the possibility to perform conversion maneuver in a civil tiltrotor aircraft while being guided by the Air Traffic Control (ATC). Moreover, conversion from helicopter to airplane configuration and vice versa is characterized by high structural loads, both on rotor and airframe (Refs. 4, 5).

To increase safety during conversion maneuver, it is necessary to ensure Level 1 handling qualities and limit the structural loads; this can be achieved by an automatic conversion system. Such systems are envisioned in the patents filed by (Refs. 7, 8). Flight envelope protection can be incorporated in automatic nacelle angle conversion system to keep the aircraft within the conversion corridor. An optimal velocity−nacelle angle combination can be predetermined based on safe length (equal distance) from upper and lower boundaries of the conversion corridor, minimizing aeroelastic instabilities and structural loads etc. This optimal conversion maneuver is then either displayed to the pilot in order to assist in manual conversion and/or automatically performed by Flight Control System (FCS). A preliminary work on optimization of tiltrotor conversion maneuver is presented in (Ref. 9).

In order to design an automatic conversion system, a detailed flight dynamics model is required that can imitate the behavior of real aircraft. Such model give insight into dynamics of the aircraft and can be used in piloted simulations and Flight Control System (FCS) design. In context of the current study, a model stitching technique (Ref. 10) is employed for modeling the flight dynamics of a tiltrotor in the conversion corridor, that falls into the category of quasi-Linear Parameter Varying models (Ref. 11). In this technique, the linearized discrete state-space models are *stitched* together to obtain a continuous and time varying model. A low order qLPV model for NASA's LCTR2 (Large Civil Tiltrotor, 2nd generation) was developed in (Ref. 12) for the purpose of handling quality analyses in hover and low speed. Most recently, qLPV model for a tiltrotor aircraft was developed by Berger et al. (Ref. 13). In both studies, the linear state-space models were dependant on two scheduling parameters (velocity V and nacelle angle β_i). In the current study, however, the models are parameterized using four scheduling parameters (altitude h, nacelle angle β_i, wing flap angle δ_f and velocity V).

In this research, a gain scheduled tracking controller based on optimal control theory is developed to perform the conversion maneuver. The controller is designed using the qLPV model and is utilized to perform a constrained multi-objective nonlinear optimization to identify the optimal conversion maneuver.

The paper is organized as follows. First, the development of qLPV model is described in detail. Second, the control synthesis for the conversion maneuver and the stability challenges associated with LPV control are discussed. Next, the optimization technique is outlined and the corresponding results are presented. Lastly, a brief conclusion and plans for future research are presented.

quasi-LINEAR PARAMETER VARYING (qLPV) MODEL

Theory

Linear state-space models that depend continuously on time varying scheduling parameters $\rho(t)$ are known as Linear Parameter Varying (LPV). In the LPV modeling approach, the linear state-space models and corresponding trim data, obtained at discrete trim points, are interpolated through lookup tables as function of the scheduling parameters. The LPV model is defined as (Ref. 11):

$$\dot{\mathbf{x}}(t) = \mathbf{A}(\rho(t))\,\mathbf{x}(t) + \mathbf{B}(\rho(t))\,\mathbf{u}(t) \tag{1}$$

A quasi-LPV (qLPV) model is a particular case of LPV model, where a subset of scheduling parameters is also state of the system. If the state vector $\mathbf{x}(t)$ can be decomposed into scheduling states $\mathbf{z}(t)$ and non-scheduling states $\mathbf{w}(t)$, then the qLPV model is defined as:

$$\begin{bmatrix} \dot{\mathbf{z}}(t) \\ \dot{\mathbf{w}}(t) \end{bmatrix} = \mathbf{A}(\rho(t)) \begin{bmatrix} \mathbf{z}(t) \\ \mathbf{w}(t) \end{bmatrix} + \mathbf{B}(\rho(t))\,\mathbf{u}(t) \tag{2}$$

In the above equation, scheduling parameter vector is composed of scheduling states and exogenous scheduling variables $\rho(t) = [\,\mathbf{z}(t) \quad \xi(t)\,]$.

An extension to the qLPV model is proposed by Tischler (Ref. 10), the *stitched* model, where the rigid body nonlinear equation of motion including the nonlinear gravitational forces are combined with the LPV model of remaining degrees-of-freedom to obtain a continuous and time varying quasi-nonlinear model.

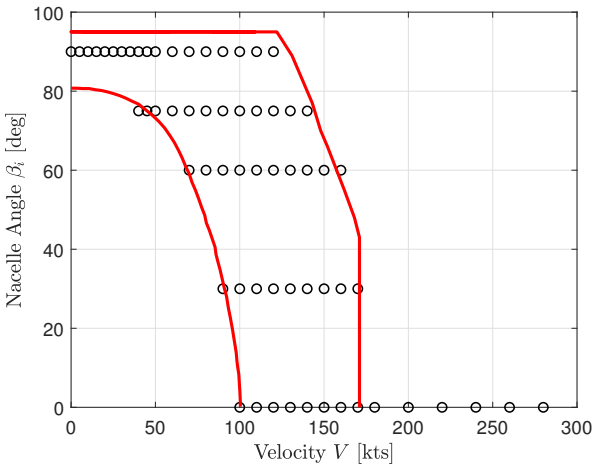

Fig. 2. XV-15 linear state-space models and conversion corridor

Linear Models

Discrete aeroelastic linear models of XV-15 are obtained in the simulation tool MASST (Modern Aeroservoelastic State Space Tools), developed at Politecnico di Milano (Refs. 14, 15). Rotor aeroelastic models in MASST are obtained from CAMRAD/JA (Ref. 16) using data published in (Refs. 17,18). The flexible airframe is included using aeroelastic NASTRAN model.

Linear state-space models and corresponding trim data are obtained spanning the conversion corridor. Additionally, the models are obtained at four wing flap δ_f settings (δ_f = [0 20 40 75] deg.) and at two altitudes (h = [0 10000] ft). The grid of linear state-space models computed for each wing flap setting and altitude, is shown in Figure 2. Rectangular regular grid is generated by clipping and keeping the edge models.

The linear state-space models contain 85 states:

- Rigid body states (9)
- Wing bending 1st mode and it's time derivative (2)
- Three blade bending modes in multi-blade coordinates (one collective and two cyclic) for each rotor and their time derivative (36)
- Two blade torsional modes in multi-blade coordinates (one collective and two cyclic) for each rotor and their time derivative (24)
- Two gimbal states in multi-blade coordinates (two cyclic) for each rotor and their time derivative (8)
- three inflow states (average, cosine and sine) for each rotor, based on the classical Pitt Peters model (Ref. 19) (6)

And 10 inputs:

- Collective pitch θ_0 for each rotor (2)
- Lateral and Longitudinal cyclic pitch (θ_{1c}, θ_{1s}) for each rotor (4)
- Aerodynamics control surface deflections (δ_f, δ_e, δ_r, δ_a) (4)

qLPV Model

The qLPV model is developed by scheduling the linear state-space models with $\rho(t) = \begin{bmatrix} h & \beta_i & \delta_f & V \end{bmatrix}$. Figure 3 presents the qLPV model structure (adapted from (Ref. 13)). The model is quasi-LPV because V and h are dependent on the states of linear system ($V = \sqrt{u^2+w^2}$ and $\dot{h} = u\sin\theta - w\cos\theta$). This endogenous state dependency may result in nonlinear feedback.

Referring to Figure 3, the lookup tables of the aircraft trim states, trim control inputs and stability and control derivatives are implemented based on the linear state-space models and trim data. These models and corresponding trim data are computed from a nonlinear model of the aircraft by CAMRAD/JA. The perturbation in states $\Delta\mathbf{x} = \mathbf{x}(\rho(t)) - \mathbf{x}_{trim}(\rho(t))$ and controls $\Delta\mathbf{u} = \mathbf{u} - \mathbf{u}_{trim}(\rho(t))$ are multiplied by the interpolated rigid body stability and control derivatives and mass matrix to obtain perturbed aerodynamic and control forces and moments. Additionally, the state and control perturbation are multiplied by higher order state-space model to get the higher order state derivatives. Note that in both cases, rigid body and higher order models, the interpolation is based on low-pass filtered velocity $V_{filtered}$ (with a cutoff frequency of $\omega_f = 0.2$ rad/s) to ensure constant state derivative values for short term motion. It will be shown, in the next section, that this filtering operation is crucial to assume global stability of the qLPV model. The perturbed aerodynamic forces and moments are then summed with the nonlinear gravitational forces and passed through nonlinear equations of motion to obtain rigid body state derivatives. Aircraft states are obtained by integrating the rigid body state derivatives combined with the higher order state derivatives.

It is important to mention here that the Coriolis terms (e.g., $Z_q = Z_q - u_{trim}q$) and linearized gravity terms (e.g., $g\theta$) are removed from state matrix $\mathbf{A}$. Moreover, because wing flap angle δ_f is one of the scheduling parameter, the control derivatives associated with δ_f in control matrix $\mathbf{B}$ are set to zero. The effect of change in δ_f is preserved implicitly in the model by the variation in trim states and controls.

Actuator Dynamics

A first order actuator dynamics model, Eq. 3, is also implemented. Time constants for different actuator types are presented in Table 1. Saturation limits for each control input are also listed in Table 1, that are obtained from (Ref. 20) .

$$G_{act}(s) = \frac{1}{\tau s + 1} \tag{3}$$

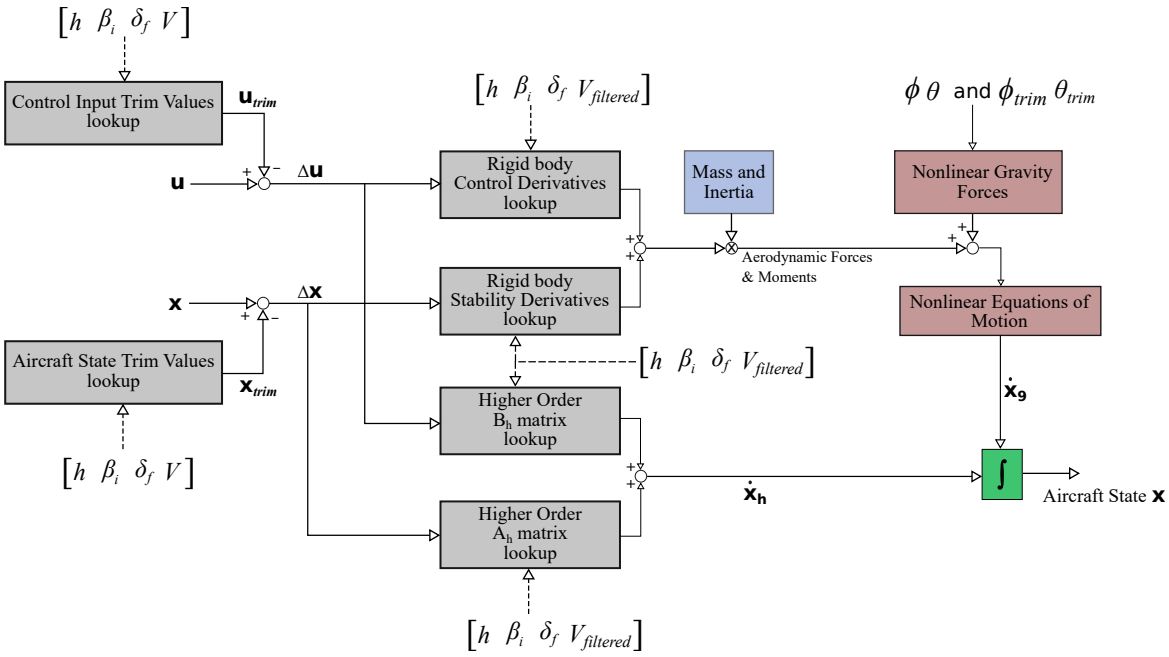

Fig. 3. qLPV model structure for XV-15

Table 1. Actuator time constant and saturation limits

Actuator Type	Control	Time Constant τ [s]	Saturation Limit [deg.]	Positive Deflection
Rotor	Collective θ_0		[0 49]	Up
Controls	Longitudinal cyclic θ_{1s}	0.040	[-10 10]	Forward
	Lateral cyclic θ_{1c}		[-10 10]	Right
Aerodynamic	Flap δ_f	0.500	[0 75]	Trailing edge down
Surfaces	Elevator δ_e		[-20 20]	Trailing edge down
	Aileron δ_a	0.077	[-13.8 23.8]	Right trailing edge down
	Rudder δ_r		[-20 20]	Right

Model Validation via Time Response Analysis

As an example of qLPV model validation, Figures 4 – 6 show the Stability and Control Augmentation System (SCAS) OFF response to a longitudinal stick input in helicopter, airplane and conversion mode, respectively. Figures 4 and 5, show the correlation of time histories with NASA's Generic Tilt-Rotor Simulation (GTRS) model (Ref. 21). In Figure 6, the correlation is shown with the Flightlab model of XV-15 (Ref. 3). In all the figures, qLPV model shows fairly good agreement with GTRS and Flightlab models. The small differences can be explained by the fact that a slightly different gearing ratio for longitudinal stick to elevator K_E is used, when generating the linear state-space models from CAMRAD/JA. $K_E = 4.735$ deg/in. is used, however, in GTRS and Flightlab models $K_E = 4.16$ deg/in.

CONTROL SYNTHESIS

A gain scheduled linear quadratic tracker with integrator (LQTI) is designed for XV-15 to perform the automatic conversion maneuver.

Linear Quadratic Tracker with Integrator (LQTI)

Consider an input vector $\mathbf{u}(t) \in \Re^m$ and a state vector $\mathbf{x}(t) = \begin{bmatrix} x_r(t) & e_t(t) & \int e_t(t)\,dt \end{bmatrix}^T$, where $x_r(t) \in \Re^n$ are the regulating states and $e_t(t) \in \Re^l$ are the tracking error states, then the augmented linear state-space model is given as (Ref. 22):

$$\begin{bmatrix} \dot{x}_r(t) \\ \dot{e}_t(t) \\ e_t(t) \end{bmatrix} = \begin{bmatrix} \mathbf{A} & \mathbf{0} \\ \mathbf{A}_{\text{add}} & \mathbf{0} \end{bmatrix} \begin{bmatrix} x_r(t) \\ e_t(t) \\ \int e_t(t)\,dt \end{bmatrix} + \begin{bmatrix} \mathbf{B} \\ \mathbf{0} \end{bmatrix} \mathbf{u}(t)$$

$$\mathbf{A}_{\text{add}} = \begin{bmatrix} \mathbf{0} & I_{l\times 1} \end{bmatrix} \tag{4}$$

The performance index to be minimized is (Ref. 23):

$$J = \frac{1}{2}\int_0^\infty \{x^T(t)Qx(t) + u^T(t)Ru(t)\}dt \tag{5}$$

where $Q \in \Re^{(n+l)\times(n+l)}$ is a real symmetric positive semi-definite states weighting matrix and $R \in \Re^{(m)\times(m)}$ is a real

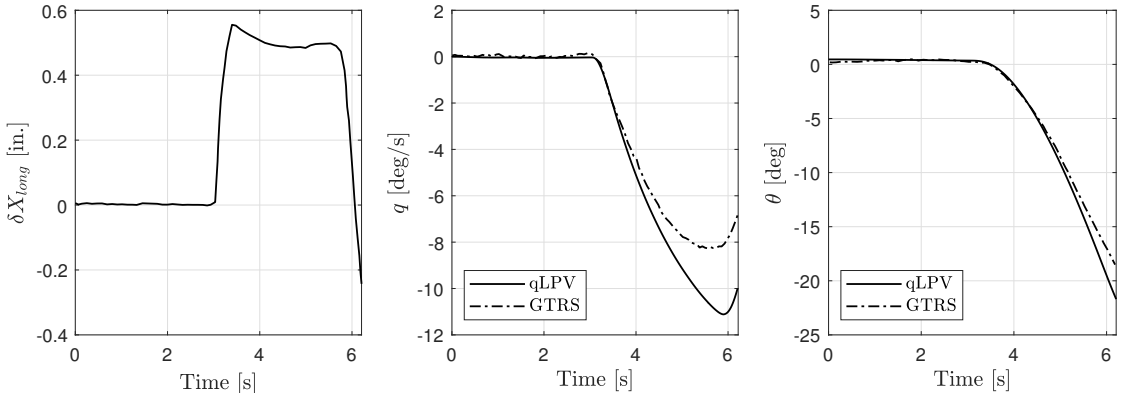

Fig. 4. Time history correlation of SCAS OFF pitch response in helicopter mode at 0 kts

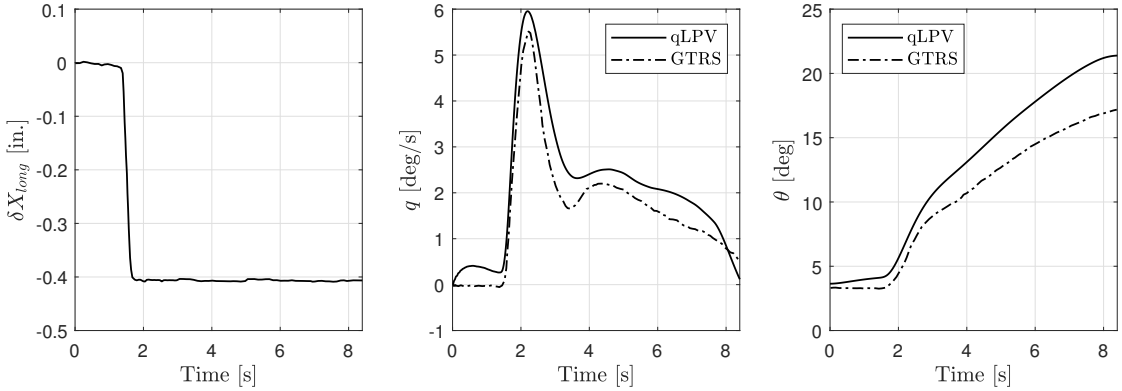

Fig. 5. Time history correlation of SCAS OFF pitch response in airplane Mode at 175 kts

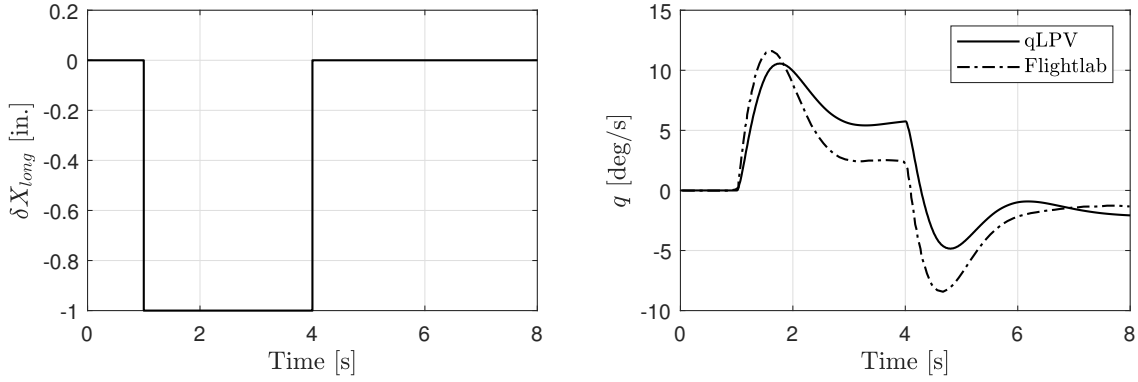

Fig. 6. Time history correlation of SCAS OFF pitch response in conversion mode ($\beta_i = 60^0$) at 120 kts

symmetric positive definite control input weighting matrix. Now the control input of the LQTI controller is calculated as:

$$\begin{aligned} \mathbf{u}(t) &= -K\mathbf{x}(t) \\ K &= \begin{bmatrix} K_r & K_t & K_i \end{bmatrix} \end{aligned} \tag{6}$$

The control gain K consists of regulating gain K_r, tracking gain K_t and integral gain K_i. The LQTI controller is designed for qLPV model spanning the entire grid of linear state-space models, therefore, the control gain is also scheduled $K(\rho(t))$. Figure 7 shows the control system block diagram of LQTI implemented on qLPV model of XV-15.

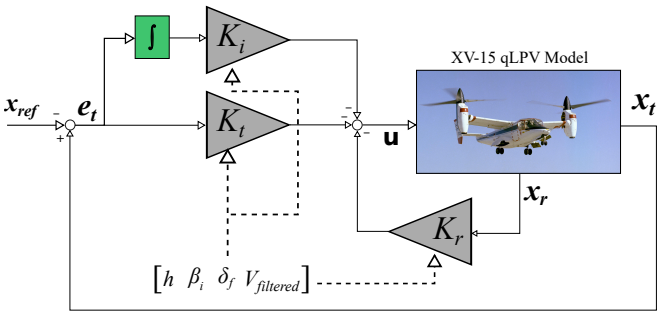

Fig. 7. Block diagram of LQ tracker with integrator

LPV Stability

Two main concepts of stability can be associated with LPV systems; 1) stability at constant scheduling trajectory (frozen or local stability) and 2) stability along varying $\rho(t)$ (global stability) (Ref. 24). Frozen stability does not imply global stability, however, if the system is locally stable then global stability can be ensured by slow variations of $\rho(t)$. That is, if frozen stability is defined as:

$$\mathrm{Re}\left[\lambda_i\left(A(\rho_j) - B(\rho_j)K(\rho_j)\right)\right] < 0 \qquad \forall \rho_j \tag{7}$$

then the global stability can be defined as:

$$\begin{aligned} &\mathrm{Re}\left[\lambda_i\left(A(\rho(t)) - B(\rho(t))K(\rho(t))\right)\right] < 0 \\ &\text{iff } \dot{\rho}(t) \text{ is very small.} \end{aligned} \tag{8}$$

In the current work, global stability is assumed by scheduling the control gain matrix $K(\rho(t))$ (also $\mathbf{A}$ and $\mathbf{B}$, as described in the previous section) based on low-pass filtered velocity $V_{filtered}$. This does not guarantee global stability and the assumption may not hold for rapid maneuvers (high nacelle angle tilt rates or excessive acceleration).

Automatic Conversion Maneuver

Results of a conversion maneuver along the center of conversion corridor are presented here. Reference velocity-nacelle angle trajectory is followed, with a constant reference altitude of 0 ft. The tracking states, velocity and altitude $x_t = \begin{bmatrix} V & h \end{bmatrix}$, are not part of the original state-space models generated through MASST. The tracking states are augmented into the original system by applying coordinate transformation using trim pitch angle θ_{trim} and trim angle of attack $\alpha_{trim} = \tan^{-1}\frac{w_{trim}}{u_{trim}}$ as follows;

$$\begin{aligned} \dot{h}(t) &= \mathbf{H}(\rho)\mathbf{x}^T(t) \\ &= \begin{bmatrix} \sin(\theta_{trim}(\rho)) & 0 & -\cos(\theta_{trim}(\rho)) & \mathbf{0} \end{bmatrix}\mathbf{x}^T(t) \\ V(t) &= \mathbf{C}(\rho)\mathbf{x}^T \\ &= \begin{bmatrix} \cos(\alpha_{trim}(\rho)) & 0 & -\sin(\alpha_{trim}(\rho)) & \mathbf{0} \end{bmatrix}\mathbf{x}^T(t) \end{aligned} \tag{9}$$

It should be noted, however, that this linear transformation is only applied to augment the state matrix, nonlinear $\dot{h} = u\sin\theta - w\cos\theta$ and $V = \sqrt{u^2+w^2}$ are used as feedback. Then the LPV model of Eq. (1) augmented with Eqs. (4) & (9) becomes:

$$\begin{Bmatrix} \dot{\mathbf{x}}(t) \\ \dot{e}_h(t) \\ \dot{e}_V(t) \\ e_h(t) \\ e_V(t) \end{Bmatrix} = \begin{bmatrix} \mathbf{A}(\rho(t)) & 0 & 0 & 0 & 0 \\ \mathbf{H}(\rho(t)) & 0 & 0 & 0 & 0 \\ \mathbf{C}(\rho(t)) & 0 & 0 & 0 & 0 \\ \mathbf{0} & 1 & 0 & 0 & 0 \\ \mathbf{0} & 0 & 1 & 0 & 0 \end{bmatrix} \begin{bmatrix} \mathbf{x}(t) \\ e_h(t) \\ e_V(t) \\ \int e_h(t)\,dt \\ \int e_V(t)\,dt \end{bmatrix} + \begin{bmatrix} \mathbf{B}(\rho(t)) \\ 0 \\ 0 \\ 0 \\ 0 \end{bmatrix} \mathbf{u}(t) \tag{10}$$

State and control weighting matrices (Q and R) are diagonal matrices and their diagonal elements are presented in Table 2. For all the discrete linear state-space models (grid of aircraft configurations and flight conditions $[h \times \beta_i \times \delta_f \times V]$), same Q and R matrices are used to compute the control gains. Very high weights are selected for lateral-directional states and controls, as the conversion maneuver is essentially a longitudinal motion. As mentioned in the previous section, the wing flap deflection is one of the scheduling parameter and is not used as an input therefore, the weight for wing flap deflection δ_f is also selected to be very high. Instead, wing flap deflection is scheduled with velocity as suggested by (Ref. 25), see Figure 8.

It should be noted that in XV-15 the gearing ratios from pilot stick inputs to rotor controls are function of nacelle angle, and the rotor controls are progressively phased out as the aircraft converts from helicopter to airplane mode. However, in the current study all control inputs are used throughout the conversion maneuver.

Figures 9–15 present various results obtained by performing the conversion maneuver along the center of conversion corridor. The conversion maneuver is performed at a constant

Table 2. Diagonal elements of Q and R weighting matrices

States	Q	Control Inputs	R
u	0.1	θ_{0R}	25000
w	0.1	θ_{1cR}	10^6
q	95000	θ_{1sR}	25000
θ	95000	θ_{0L}	25000
Lateral-Directional States	10^6	θ_{1cR}	10^6
Wing Bending & Rotor States	20	θ_{1sL}	25000
Wing Bending & Rotor States Derivative	0	δ_f	10^6
e_h	0.5	δ_e	9000
e_V	0.1	δ_a	10^6
$\int e_h dt$	2.5	δ_r	10^6
$\int e_h dt$	5		

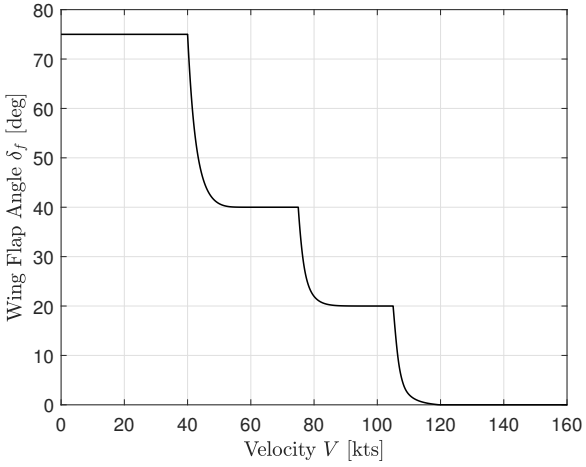

Fig. 8. Wing flap deflection with velocity

acceleration $\dot{V} = 4$ kts/s and at a nacelle angle conversion rate $\dot{\beta} = 3$ deg/s for nacelle angles greater than 75° and $\dot{\beta} = 8$ deg/s for nacelle angles less than 75°.

Figure 9 presents the conversion trajectory, whereas time histories of velocity, nacelle angle and altitude are presented in Figure 10. The LQTI controller performs very well in following the reference velocity and keeping the altitude constant. The change in altitude during the complete conversion maneuver is within ±10 ft. Figure 11 presents the evolution of aircraft pitch rate and pitch angle during the conversion maneuver.

The variation of control inputs is shown in Figure 12. As mentioned previously, that no control is phased out as a function of nacelle angle, rather all the controls are utilized during the conversion maneuver. The longitudinal cyclic θ_{1s} and elevator deflection δ_e do saturate for small period of time. The high demand on longitudinal inputs occur when nacelle angle starts to tilt from $\beta_i = 60°$ to 0°.

Figures 13 and 14 show the out-of-plane rotor flapping states

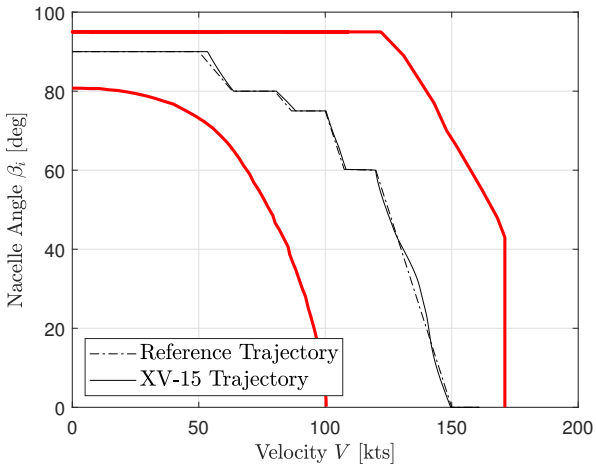

Fig. 9. Conversion maneuver along the center of conversion corridor

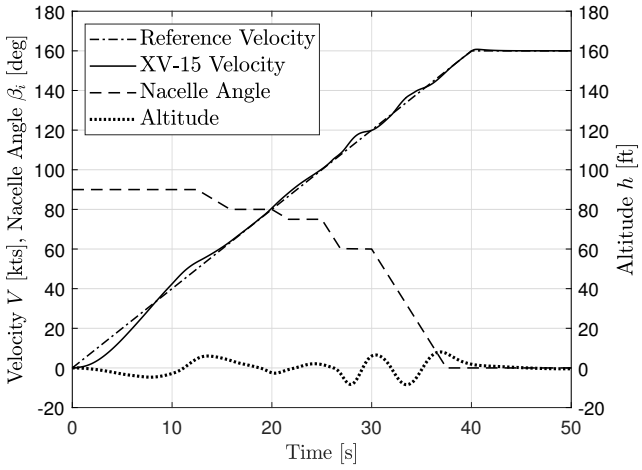

Fig. 10. Time history of velocity, nacelle angle and altitude during centered conversion maneuver

of right rotors during the conversion maneuver. Flapping of elastic rotor is within 1.5°, see Figure 13. Interestingly, the conversion maneuver which essentially is a longitudinal motion, causes a lateral flapping β_{1s}. This lateral flapping is induced by the nacelle conversion due to the gyroscopic effect. Figure 14 shows the longitudinal and lateral gimbal of right rotor. Maximum longitudinal gimbal β_{Gc} occurs when maximum longitudinal cyclic input is applied, see also Figure 12.

Lastly, Figure 15 shows the deflection of right wing pylon about three axes. The axes system is parallel to the body axes (X forward towards nose, Y towards right wing and Z pointing downwards) and is placed at the tip of wing pylon. The main deflection is about X axis, the out-of-plane deflection. There is a small deflection about Y axis, the torsional deflection and about Z-axis there is almost no deflection.

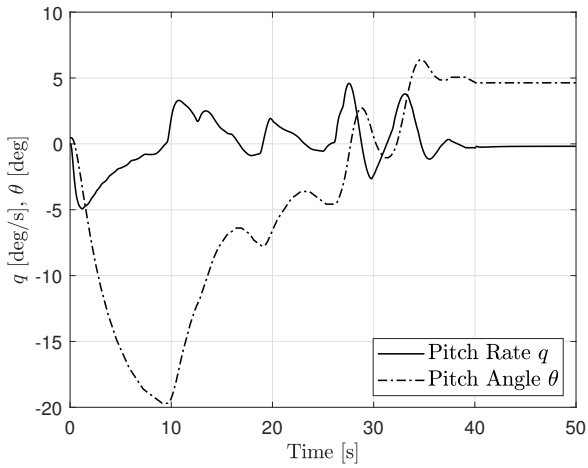

Fig. 11. Aircraft pitch rate and pitch angle during centered conversion maneuver

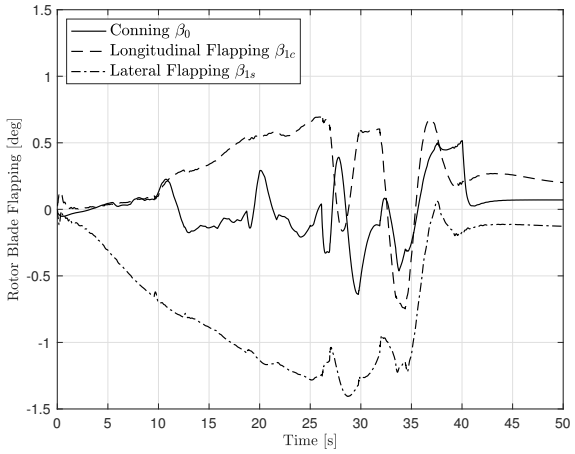

Fig. 13. Out-of-plane right rotor flapping during centered conversion maneuver (at rotor tip)

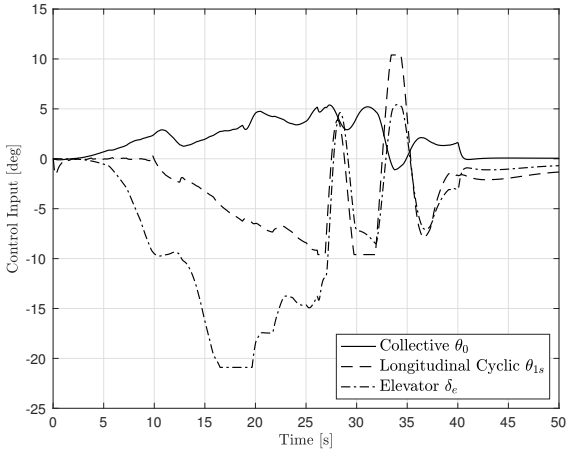

Fig. 12. Control inputs to perform centered conversion maneuver

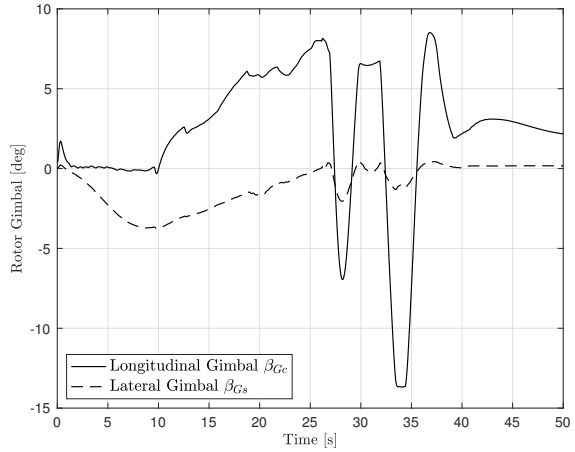

Fig. 14. Right rotor gimbal during centered conversion maneuver

CONVERSION MANEUVER OPTIMIZATION

Any conversion maneuver that is within the conversion corridor enables the tiltrotor to transition from helicopter mode to airplane mode and vice versa. However, some conversion maneuvers are difficult to fly than the others. For example, flying at high nacelle angle conversion rate, the handling quality ratings degrade significantly that may lead to Pilot Induced Oscillations (PIO) (Ref. 3). Moreover, some conversion maneuvers require high control effort that can cause high rotor blade flapping and gimbal deflections. Therefore, in the current research an optimization is performed to recommend an optimal conversion maneuver trajectory.

A total of 119 conversion maneuvers are performed at two accelerations $\dot{V} = \begin{bmatrix} 3 & 4 \end{bmatrix}$ kts/s. The nacelle angle conversion rate is same as in the previous section. Complete conversion from helicopter mode to airplane mode, from V = 0 kts to V = 170 kts, is accomplished through a set of discrete nacelle angle and velocity combinations. Figure 16 shows all the reference trajectories that are flown to identify the optimal conversion trajectory.

An optimal conversion maneuver is selected from the above set that minimizes a certain objective function. Based on the results presented in the previous section (Figures 11 and 14), the objective function is defined as follows:

$$\min_{V,\beta_i} J = \frac{1}{T_s}\int_0^{T_s}\left(100q^2 + 100\beta_{Gc}^2\right)dt + \left(\frac{V - V_{center}}{V_{center}}\right)^2_{\forall\beta_i} \quad (11)$$

The objective function is a sum of integral of weighted states and normalized distance from conversion corridor center. The optimal conversion maneuver is selected to be the one that has minimum pitch rate, minimum longitudinal gimbal deflection

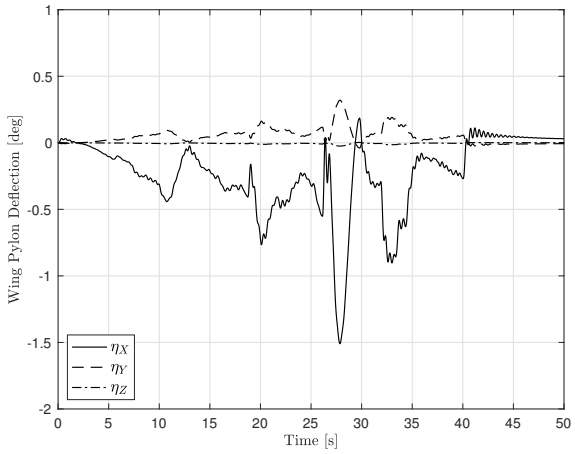

Fig. 15. Right wing pylon tip bending during centered conversion maneuver

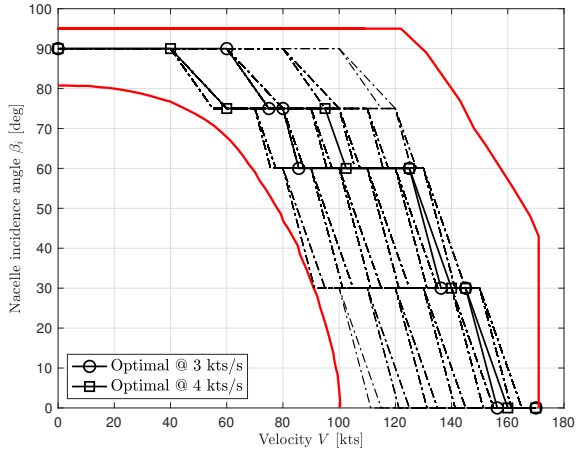

Fig. 16. Conversion maneuver trajectories

and that is flown close to the center of conversion corridor. The integral of weighted sum of states is normalized by final simulation time T_f. Figure 16 also show the optimal conversion maneuvers at two accelerations that minimize the above stated objective function.

Figure 17 present the time histories of velocity, nacelle angle and altitude for optimal conversion maneuvers at two accelerations. With $\dot{V}$ = 3 kts/s, total time to reach the final velocity of 170 kts is 55 seconds compared to conversion at $\dot{V}$ = 4 kts/s, where time to reach 170 kts is 42 seconds.

The pitch rate and pitch angle during the optimal conversion maneuver are presented in Figure 18. At $\dot{V}$ = 4 kts/s, there is not much of an improvement in pitch rate and pitch angle when compared with the results of Figure 11. However, the magnitude of pitch rate and pitch angle decreases at low acceleration conversion maneuver $\dot{V}$ = 3 kts/s.

The evolution of control inputs during the optimal conversion maneuver is shown in Figure 19. For optimal conversion trajectory, the magnitude of control demand has decreased when compared with the control demand during conversion maneuver along the center of conversion corridor. Additionally, control demand further decreases at low acceleration conversion maneuver.

Lastly, longitudinal and lateral gimbal deflection of right rotor is shown in Figure 20. A remarkable reduction in longitudinal rotor gimbal deflection is observed, that was one of the objective of optimization.

CONCLUSIONS

A high order quasi-Linear Parameter Varying (qLPV) model is developed for XV-15. The qLPV model is scheduled using four dimensional lookup tables: altitude, nacelle angle, wing flap deflection and aircraft velocity. Actuator dynamics are also incorporated in the flight dynamics model. With the aim of performing automatic conversion maneuver, control synthesis of a gain scheduled linear quadratic tracker with integrator is presented.

It is demonstrated that utilizing the same controller, different conversion trajectories within the conversion corridor have different dynamic behavior, in terms of aircraft states and control input demand. Optimal conversion trajectories can be computed that minimize certain states and required control effort. In the current research, optimal conversion maneuvers were computed at two different accelerations, $\dot{V}$ = 3 kts/s and $\dot{V}$ = 4 kts/s, that minimize the aircraft pitch rate and longitudinal rotor gimbal deflection and are flown away from the conversion corridor boundaries. Better performance is observed for conversion at $\dot{V}$ = 3 kts/s. Conversion maneuver is completed in less than a minute in both cases.

At this moment, the controller is designed to perform an automatic conversion maneuver. That is, during conversion from helicopter to airplane mode, follow a reference velocity while maintaining constant altitude. In the future, higher order states can be incorporated in the control synthesis, for example, active control for load alleviation during automatic conversion maneuver and other flying qualities critical maneuvers.

It is also shown that in order to ensure global stability of LPV control, the change in scheduling parameter must be small. Therefore, the control gains along with the linear state-space models are scheduled using low-pass filtered velocity. However, this does not necessarily guarantee the global stability and therefore a robust control approach needs to be developed for qLPV systems. Additionally, a better control allocation technique must be defined, in order to use the redundant control inputs effectively in all three configurations: helicopter, airplane and conversion mode. Future work will extend to the development of robust nonlinear control synthesis for qLPV systems and effective control allocation techniques for tiltrotor aircraft.

Author contact: Hafiz Noor Nabi hafiznoor.nabi@polimi.it & h.n.nabi@tudelft.nl

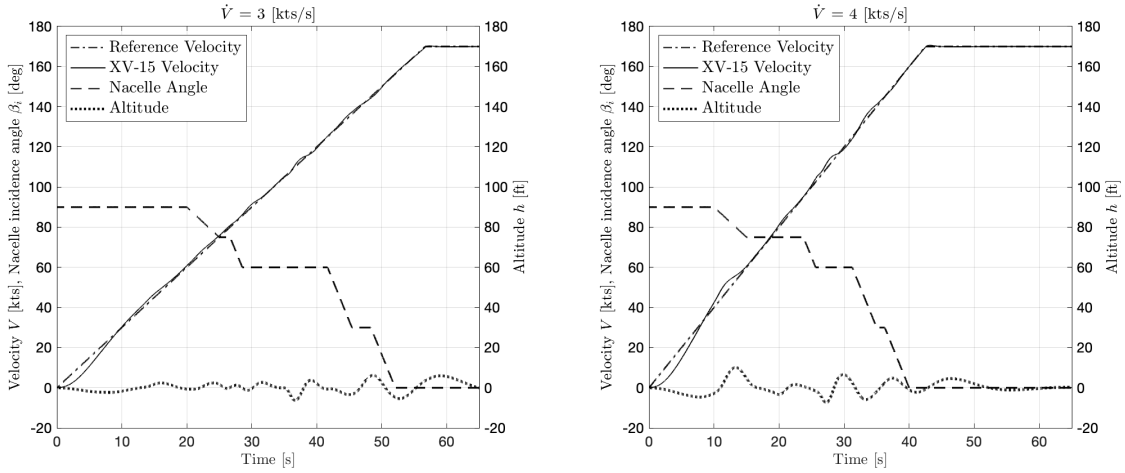

Fig. 17. Time history of velocity, nacelle angle and altitude during optimal conversion maneuver. Left: 3 kts/s, Right: 4 kts/s

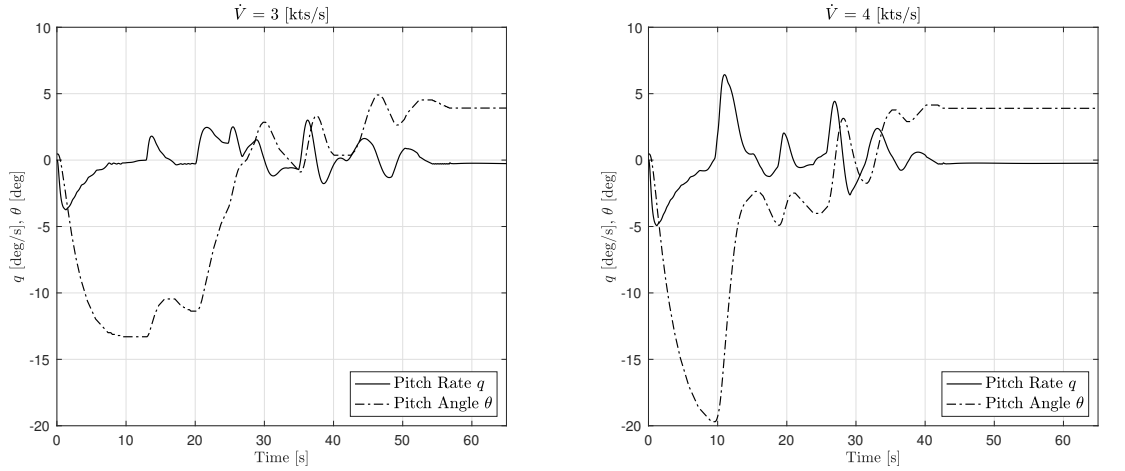

Fig. 18. Aircraft pitch rate and pitch angle during optimal conversion maneuver. Left: 3 kts/s, Right: 4 kts/s

ACKNOWLEDGMENTS

The NITROS (Network for Innovative Training on ROtorcraft Safety) project has received funding from the European Union's Horizon 2020 research and innovation program under the Marie Skodowska-Curie grant agreement # 721920.

REFERENCES

[1]Renaud, J., Huber, H., and Venn, G., "The Eurofar Program – An European Overview on Advanced VTOL Civil Transportation System," 17th European Rotorcraft Forum, Berlin, Germany, September 1991.

[2]Rollet, P., "RHILP – A Major Step for European Knowledge in Tilt-Rotor Aeromechanics and Flight Dynamics," *Air & Space Europe*, Vol. 3, (3-4), May–August 2001, pp. 152–154.
doi: 10.1016/S1290-0958(01)90080-2

[3]Padfield, G. D., *Helicopter Flight Dynamics: Including a Treatment of Tiltrotor Aircraft*, John Wiley & Sons, West Sussex, UK, 2018, pp. 633 & 670–672.

[4]King, D. W., Dabundo, C., Kisor, R. L., and Agnihotri, A., "V-22 Load Limiting Control Law Development," American Helicopter Society 49th Annual Forum, St. Loius, Missouri, May 1993.

[5]Manimala, B., Padfield, G. D., Walker, D., Naddei, M., Verde, L., Ciniglio, U., Rollet, P., and Sandri, F., "Load Alleviation in Tilt Rotor Aircraft through Active Control; Modeling and Control Concepts," *The Aeronautical Journal*, Vol. 108, (1082), April 2004, pp. 169–184.
doi: 10.1017/S0001924000000087

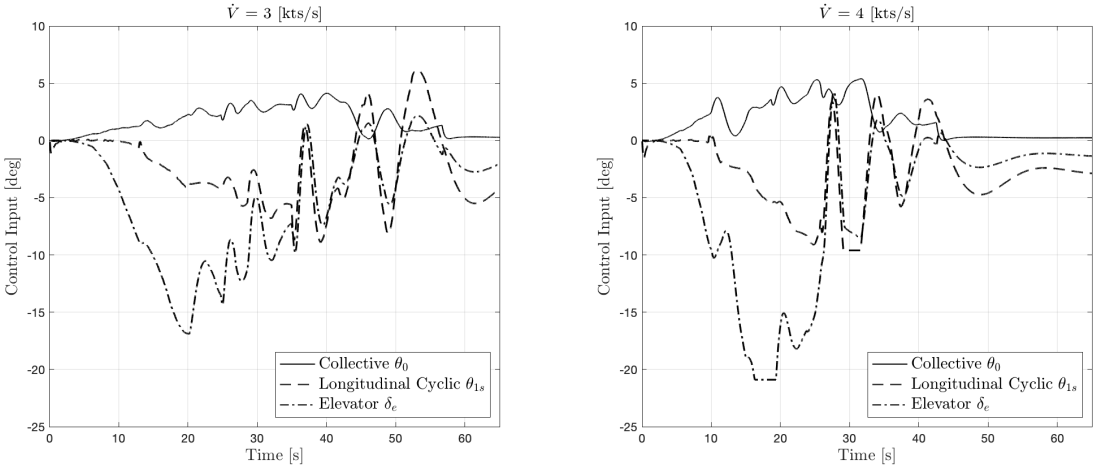

Fig. 19. Control inputs to perform optimal conversion maneuver. Left: 3 kts/s, Right: 4 kts/s

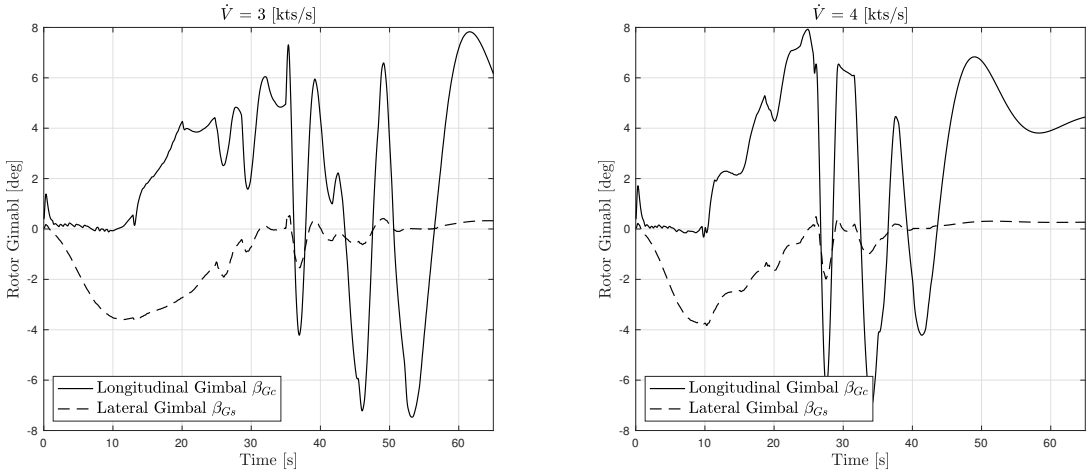

Fig. 20. Right rotor gimbal during optimal conversion maneuver. Left: 3 kts/s, Right: 4 kts/s

[6]Maisel, M., "NASA/Army XV-15 Tilt Rotor Research Aircraft Familiarization Document," NASA TM X–62,407, 1975.

[7]King, D. W. and Shultz, P. M., "Multi-Mode Tiltrotor Nacelle Control System with Integrated Envelope Protection," US Patent No. 6644588 B2, Nov. 11, 2003.

[8]Kowalski, J., Grill, I., and Seminole, "Adaptable Automatic Nacelle Conversion for Tilt Rotor Aircraft," US Patent No. 9377784 B2, Jun. 28, 2016.

[9]Righetti, A., Muscarello, V., and Quaranta, G., "Linear Parameter Varying Models for the Optimization of Tiltrotor Conversion Maneuver," American Helicopter Society 73rd Annual Forum, Fort Worth, Texas, May 2017.

[10]Tobias, E. L. and Tischler, M. B., "A Model Stitching Architecture for Continuous Full Flight-Envelope Simulation for Fixed-Wing Aircraft and Rotorcraft from Discrete-Point Linear Models," U.S. Army AMRDEC SR RDMR–AF–16–01, 2016.

[11]Marcos, A. and Balas, G. J., "Development of Linear-Parameter-Varying Models for Aircraft," *Journal of Guidance, Control and Dynamics*, Vol. 27, (2), March–April 2004, pp. 218–228.
doi: 10.2514/1.9165

[12]Lawrence, B., Malpica, C. A., and Theodore, C. R., "The Development of a Large Civil Tiltrotor Simulation for Hover and Low-speed Handling Qualities Investigations," 36th European Rotorcraft Forum, Paris, France, September 2010.

[13]Berger, T., Juhasz, O., Lopez, M. J. S., Tischler, M. B., and Horn, J. F., "Modeling and Control of Lift Offset Coaxial and Tiltrotor Rotorcraft," 44th European Rotorcraft Forum, Delft, The Netherlands, September 2018.

[14]Masarati, P., Muscarello, V., and Quaranta, G., "Linearized Aeroservoelastic Analysis of Rotor-Wing Aircraf," 36th European Rotorcraft Forum, Paris, France, September 2010.

[15]Colombo, F., Muscarello, V., Quaranta, G., and Masarati, P., "A Comprehensive Aeroservoelastic Approach to Detect and Prevent Rotorcraft-Pilot Coupling Phenomena in Tiltrotors," American Helicopter Society 74th Annual Forum, Pheonix, Arizona, May 2018.

[16]Johnson, W., "CAMRAD/JA, A Comprehensive Analytical Model of Rotorcraft Aerodynamics and Dynamics- Volume I: Theory Manual," Johnson Aeronautics Version, 1988.

[17]Ferguson, S. W., "A Mathematical Model for Real Time Flight Simulation of a Generic Tilt-Rotor Aircraft," NASA CR 166536, 1988.

[18]Acree, C. W., "An Improved CAMRAD Model for Aeroelastic Stability Analysis of the XV-15 with Advanced Technology Blades," NASA TM 4448, 1993.

[19]Pitt, D. M. and Peters, D. A., "Theoretical Prediction of Dynamic Inflow Derivatives," 6th European Rotorcraft and Powered Lift Aircraft Forum, Bristol, England, September 1980.

[20]Marr, R. L., Willis, J. M., and Churchill, G. B., "Flight Control System Development for the XV-15 Tilt Rotor Aircraft," American Helicopter Society 32nd Annual Forum, Washington, D.C., May 1976.

[21]Ferguson, S. W., "Development and Validation of a Simulation for a Generic Tilt-Rotor Aircraft," NASA CR 166537, 1989.

[22]Jeong, J., Kim, S., and Suk, J., "Control System Design for a Ducted-Fan Unmanned Aerial Vehicle Using Linear Quadratic Tracker," *International Journal of Aerospace Engineering*, Vol. 2015, (Article ID 364926), 2015, pp. 12 pages. doi: 10.1155/2015/364926

[23]Lewis, F. L., Vrabie, D. L., and Syrmos, V. L., *Optimal Control*, John Wiley & Sons, Hoboken, New Jersey, 2012.

[24]Toth, R., *Modeling and Identification of Linear Parameter-Varying Systems*, Lecture Notes in Control and Information Sciences, Springer-Verlag Berlin Heidelberg, 2010, p. 93.

[25]Diaz, S., Mouterder, E., and Desopper, A., "Performance Code for Take-off and Landing Tilt-Rotor Procedures Study," 30th European Rotorcraft Forum, Marseilles, France, September 2004.